

Space Weathering Trends Among Carbonaceous Asteroids

Kaluna, H. M.¹, Masiero, J. R.², Meech, K. J.,¹

¹*Institute for Astronomy, University of Hawaii, 2680 Woodlawn Dr., Honolulu-HI-96822, USA*

²*Jet Propulsion Laboratory/Caltech, Pasadena, CA, USA*

kaluna@hawaii.edu, Joseph.Masiero@jpl.nasa.gov, meech@ifa.hawaii.edu

ABSTRACT

We present visible spectroscopic and albedo data of the 2.3 Gyr old Themis family and the <10 Myr old Beagle sub-family. The slope and albedo variations between these two families indicate C-complex asteroids become redder and darker in response to space weathering. Our observations of Themis family members confirm previously observed trends where phyllosilicate absorption features are less common among small diameter objects. Similar trends in the albedos of large (>15 km) and small (≤ 15 km) Themis members suggest these phyllosilicate feature and albedo trends result from regolith variations as a function of diameter. Observations of the Beagle asteroids show a small, but notable fraction of members with phyllosilicate features. The presence of phyllosilicates and the dynamical association of the main-belt comet 133P/Elst-Pizarro with the Beagle family imply the Beagle parent body was a heterogeneous mixture of ice and aqueously altered minerals.

Subject headings: main belt asteroids, carbonaceous asteroids, space weathering

1. Introduction

Space weathering studies on asteroids have primarily focused on the alteration of the silicate rich S-complex asteroids. These moderate albedo ($p_v \sim 0.22$; Mainzer et al. 2011) asteroids are known to spectrally darken, redden and have increasingly suppressed absorption bands as a function of time (Belton et al. 1992, 1994; Binzel et al. 1996; Chapman 1996). These spectral changes are attributed to the vapor deposition of sub-micron metallic iron (SMFe) particles onto grains during micrometeorite impacts and solar wind irradiation (Yamada et al. 1999; Hapke 2001; Sasaki et al. 2001; Brunetto & Strazzulla 2005). The intrinsically dark ($p_v \sim 0.06$; Mainzer et al. 2011) nature of carbonaceous material and the lack of prominent absorption features at visible and near-IR wavelengths implied space weathering trends would be difficult to identify for C-complex asteroids (Hapke 2001; Moroz et al. 1996). However, two recent studies indicate significant spectral slope variation among this class of asteroids as a function of age (Nesvorný et al. 2005; Lazzarin et al. 2006).

Principal component analyses of asteroid colors in the Sloan Digital Sky Survey (SDSS) show the mean slopes of C-complex asteroid families experience a decrease in slopes and become spectrally bluer

with age at visible wavelengths (Nesvorný et al. 2005). In contrast, a study using visible spectroscopic data from the Small Main-Belt Asteroid Spectroscopic Survey (SMASSII; Bus & Binzel 2002b), shows the spectral slopes of the C-complex asteroid population as a whole increase (redden) with age (Lazzarin et al. 2006). However, when Lazzarin et al. (2006) limit their analyses to the C-complex asteroid families they are able to reproduce the slope trends obtained by Nesvorný et al. (2005). Lazzarin et al. (2006) suggests the discrepancies between the two slope trends arise from a sampling effect where the average compositions of C-complex asteroids are not fully represented in the sampled C-complex families.

The Nesvorný et al. (2005) and Lazzarin et al. (2006) studies indicate significant evidence of space weathering trends among the C-complex asteroids, however the effects of compositional variation on these trends is still unclear. In the case of S-complex asteroids, Nesvorný et al. (2005) use the Koronis asteroid family and Karin cluster, which formed from the breakup of a Koronis family member, to study space weathering trends while avoiding the influence of compositional variation. The spectral trends of the young Karin (5 Myr; Nesvorný et al. 2002) and old Koronis asteroids (2.5 Gyr; Marzari et al. 1995) confirm that the reddening observed among the S-complex asteroids is indeed a result of space weathering and not a product of mineralogical variation. The recent discovery of a sub-family of the Themis asteroids allows a similar test to be conducted on C-complex asteroids. The Themis family (Hirayama 1918) has $\sim 4,000$ members (Milani et al. 2014) resulting from the catastrophic break up of a 390-450 km parent body asteroid 2.3 Gyr ago (Marzari et al. 1995). A recent (< 10 Mya) break up of a Themis family member ($D \sim 20$ km to 65 km in size) resulted in the formation of the Beagle family, which contains ~ 60 asteroids (Nesvorný et al. 2008). These two families are the first C-complex families identified which originate from the same parent body and provide a unique tool for assessing C-complex space weathering trends while alleviating the mineralogical variations among C-complex asteroids.

In this study we use spectroscopic and albedo data to search for space weathering trends among the Themis and Beagle asteroids. We compare these trends to those of the Veritas asteroid family, which is another young (8.3 Myr; Nesvorný et al. 2003) C-complex family. The Veritas asteroids are not related to the Themis and Beagle asteroids and allow us to assess whether differences in mineralogy affect the spectral trends in space weathering studies of C-complex asteroids.

2. Observations

In this paper, we present data for 52 main-belt asteroids belonging to the Themis, Beagle and Veritas asteroid families. Observations took place on 3.5 nights during Mar. 03, Oct. 29, Oct. 30, 2013 and Feb. 21, 2014 at the 8.2-meter Subaru telescope on Maunakea, Hawai'i (see Table 1 for log of observations). Spectroscopic data covering the $0.47 < \lambda < 0.91 \mu\text{m}$ spectral range were taken with the Faint Object Camera and Spectrograph (FOCAS). FOCAS has two $2\text{K} \times 4\text{K}$ CCDs with a total of 8 readout channels, each with 512×4176 pixels (Kashikawa et al. 2002). The spectra were recorded in channel 3 of chip 2, which has a read noise of 3.4 e⁻ and gain of 2.082 e⁻/ADU. We used the lowest resolution grating (75 gr/mm) and 2×2 binning to obtain the highest signal to noise ratio (SNR) for our targets which are dominated by relatively

small ($D < 15$ km) and faint asteroids. The resulting low resolution dispersion of $11.8 \text{ \AA}/\text{pixel}$ is ideal for detecting the shallow and broad absorption features typically seen in C-complex asteroid spectra. The SY47 order sorting filter was used to prevent higher order contamination. Observations were taken through a $1''$ wide slit, oriented to the parallactic angle, while tracking at non-sidereal rates. Due to the lack of non-sidereal guiding and to prevent drifting across the slit, integration times were limited to 600 seconds.

Family members were selected based on the dynamically derived memberships found in Nesvorný (2012). Previous studies show trends where the frequency of asteroids with absorption features varies as a function of diameter (Florczak et al. 1999; Fornasier et al. 2014), so Themis and Veritas targets were limited to members with similar diameters as Beagle targets ($D \leq 15$ km) to avoid size related variations. Nearby solar analog stars were observed at airmasses similar to the asteroids throughout the night and ThAr lamp spectra were taken at the beginning or end of each observing run for wavelength calibration.

3. Data Reduction and Analysis

Data were reduced using the Image Reduction and Analysis Facility (IRAF) V2.14 noao longslit and Subaru `focusrad` packages (Tody 1986). The reduction procedure included overscan and bias subtraction, image trimming, flattening, and cosmic ray removal for long exposure images. The `apall` package was used to perform background subtraction, extraction of the

one-dimensional and associated sigma spectra from the two-dimensional images. The sigma spectrum is produced by measuring the sigma at each wavelength in the two-dimensional image. Following extraction, data were wavelength calibrated using emission lines from the ThAr lamp spectra.

Median combined asteroid spectra were divided by nearby G2V solar analog spectra to produce reflectance spectra for each asteroid. The solar analog stars were observed close in time to the observations of each asteroid and were chosen to have an airmass difference of < 0.1 to enable extinction correction. The reliability of each solar analog star was tested by producing multiple reflectance spectra of an asteroid from multiple stars at similar airmasses. Only standard stars that produced consistent spectral shapes and slopes were used in producing reflectance spectra. Table 1 reports which solar analog stars were used to produce the reflectance spectra for each asteroid. Residual features due to incomplete removal of sky lines were removed using a median filter to search for erroneous spikes in the final reflectance spectra.

We measured slopes using the equation for the normalized reflectivity gradient S' (reported in units of $\%/1000 \text{ \AA}$), as defined by Jewitt & Meech (1986):

$$S'(\lambda_1, \lambda_2) = \left(\frac{dS/d\lambda}{S_{0.55}} \right) \quad (1)$$

where $dS/d\lambda$ is the slope of the reflectivity measured within the wavelength region between λ_1 and λ_2 . Reflectance spectra were normalized to $0.55 \mu\text{m}$ and spectral slopes were measured using a weighted linear least-squares fit to data between $0.49 < \lambda < 0.91 \mu\text{m}$. The fits were weighted using the IRAF generated sigma spectrum for each asteroid. Data shorter than $0.49 \mu\text{m}$ were not included in the fit due to potential

contamination from the UV absorption below $\sim 0.5 \mu\text{m}$ created by an Fe^{2+} intervalence charge transfer attributed to phyllosilicates (Vilas 1994; Hiroi et al. 1996). Asteroid slopes and 1-sigma uncertainties are shown in Table 2.

At large phase angles, asteroids are known to experience an increase in slopes (reddening) (Millis et al. 1976; Bowell & Lumme 1979; Lumme & Bowell 1981), however, Luu & Jewitt (1990) find that adopting phase coefficients from other C-complex asteroids does little to improve slope measurements for observations at small phase angles ($\lesssim 40^\circ$). In addition, we do not have phase reddening coefficients for most of our targets, but our observations span a small range of phase angles ($\lesssim 20^\circ$), thus no phase reddening correction was applied to our reflectance spectra.

One of the few features found in C-type spectra is a shallow ($< 5\%$) $0.7 \mu\text{m}$ absorption band created by phyllosilicates (Vilas & Gaffey 1989). To search for this feature we perform continuum removal and fit the $0.55\text{-}0.85 \mu\text{m}$ feature region with a 2nd or 3rd order polynomial. The continuum removed spectra were created by dividing the full spectrum by a linear fit to the $0.7 \mu\text{m}$ continuum shoulders ($0.52\text{-}0.54 \mu\text{m}$ and $0.86\text{-}0.88 \mu\text{m}$). The continuum removed spectra are shown in Figures 1-4. The band depth and center were determined using the reflectance value at the wavelength corresponding to the minimum of the polynomial fit. The band depth uncertainty was derived using the uncertainty in the sigma spectrum corresponding to the position of the band center and only features with band depths greater than the associated uncertainties were flagged as a detection. Band depths for objects where features were detected and sensitivity limits computed from the SNR of each spectrum are reported in Table 2.

In addition to our Subaru data, we use visible albedos derived by Masiero et al. (2011) from the Wide-field Infrared Survey Explorer (WISE) to characterize the albedo distributions of Themis, Beagle and Veritas asteroids. We used 2025, 565, and 16 Themis, Veritas and Beagle members, respectively, in our analyses but divided the data set into two size populations (cutoff = 15 km) for consistency with our Subaru data. The mean values for slope and albedo, the standard error of the mean (SEM) and the standard deviations for each family and size range are reported in Table 3. We use the SEM to quantify the variation in our estimate of the mean, and the standard deviation to quantify the dispersion in our slope and albedo distributions.

4. Results

Members of the Themis and Beagle families show a wide range of blue to red-sloped spectra (Table 2). However, $\sim 90\%$ (21 out of 23) Beagle asteroids have blue-sloped spectra, whereas 60% (13 out of 22) of the Themis asteroids are blue-sloped. These data suggest the Beagle family is dominated by B-type asteroids, which are characterized by negatively sloped (blue) spectra (Tholen 1984; Bus & Binzel 2002a). The Themis asteroids show a range of C, B, F and G spectral types (Tholen 1984), consistent with the observations of other Themis members (Florczak et al. 1999).

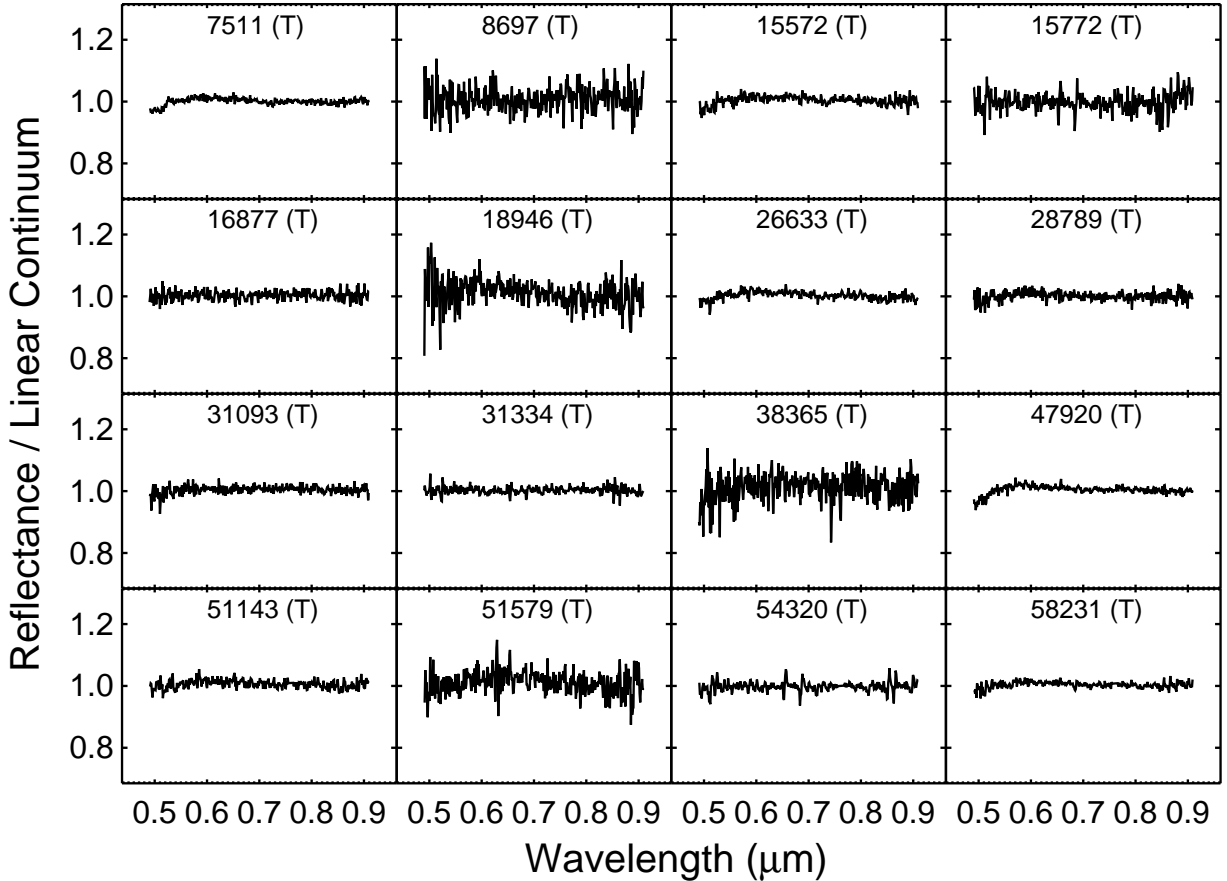


Fig. 1.— Continuum removed spectra of individual Themis (T) asteroids, where labels report the asteroid ID.

4.1. Spectral Slopes

The slope distributions for the Themis and Beagle families are shown in Figure 5. Given the larger fraction of blue sloped spectra, the weighted mean for the Beagle asteroids ($-1.280 \pm 0.003\%$ per 1000 \AA) is significantly bluer than that of the Themis asteroids ($-0.378 \pm 0.003\%$ per 1000 \AA). The difference in slopes between Themis and Beagle imply these asteroids redden by $\sim 0.9\%$ per 1000 \AA over a timespan of ~ 2.3 billion years. To test the significance of the difference in the slope distributions of the two families, we applied the Student’s T and Kolmogorov-Smirnov (KS) tests to the Themis and Beagle data sets. We find the difference in means is significant at the 2-sigma level.

The Themis asteroid 18946 is extremely red ($3.037 \pm 0.005\%$ per 1000 \AA), and is located near the outer region of the proper element distributions for the Themis family. Due to the possibility of 18946 being an interloper, we exclude 18946 from our analyses, and compute a new mean slope of $-0.505 \pm 0.003\%$

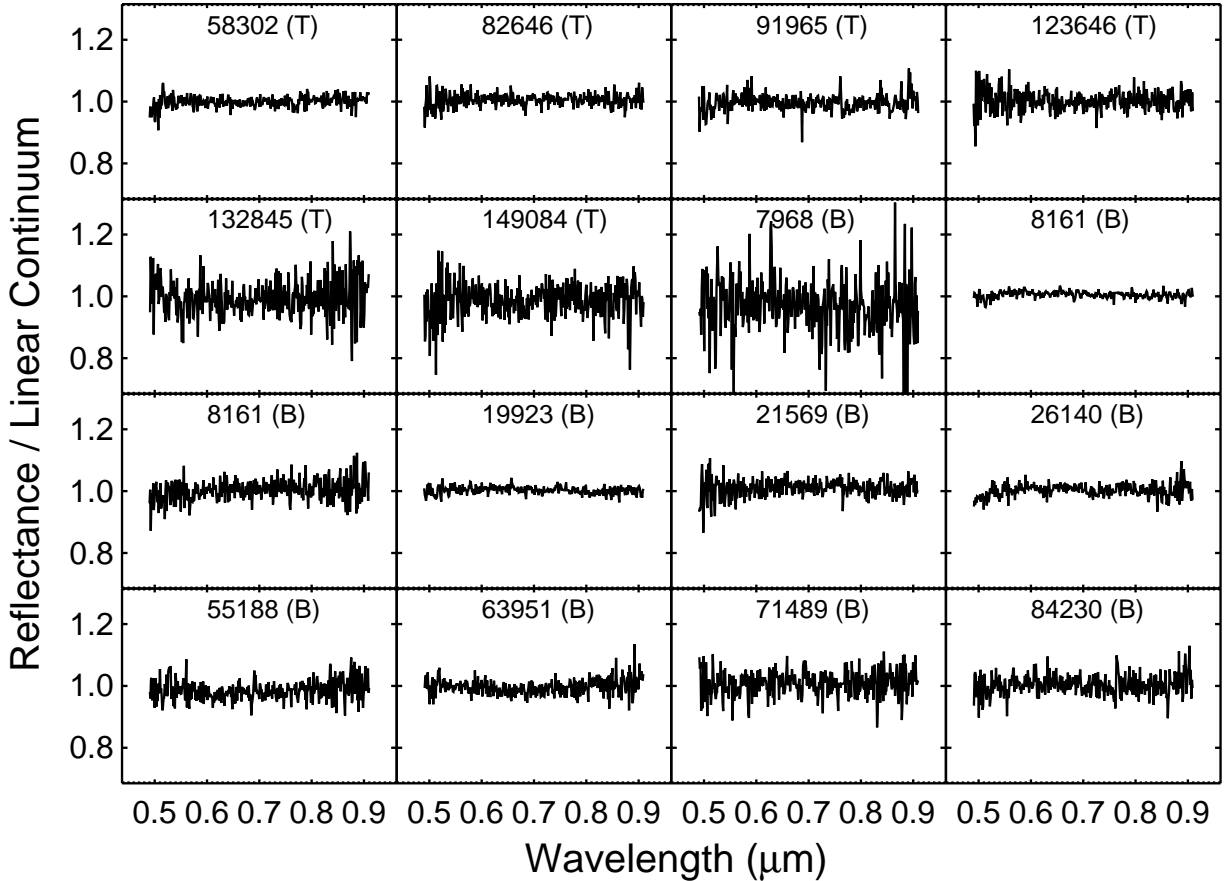


Fig. 2.— Continuum removed spectra of individual asteroids. Labels show the asteroid ID as well as family membership, where (T) and (B) are Themis, Beagle family members, respectively.

per 1000 Å for the Themis asteroids. The reduced mean equates to a slope reddening rate of $\sim 0.8\%$ per 1000 Å in ~ 2.3 billion years. After re-applying the statistical tests, the difference in means between the Themis and Beagle populations is still significant at the 2-sigma level although there is a slight drop in significance.

The Beagle asteroids 140399 and 8161 were each observed on two nights and have significantly varied spectral slopes (Table 2). Both spectra of 140399 show the asteroid is moderately blue, however spectra of 8161 are both blue and red sloped. Both spectra were taken during photometric conditions and produced using the same solar analog star, thus the large slope variation in asteroid 8161 may imply color differences across the surface of this asteroid. However, follow-up observations are needed to assess whether these trends can be reproduced.

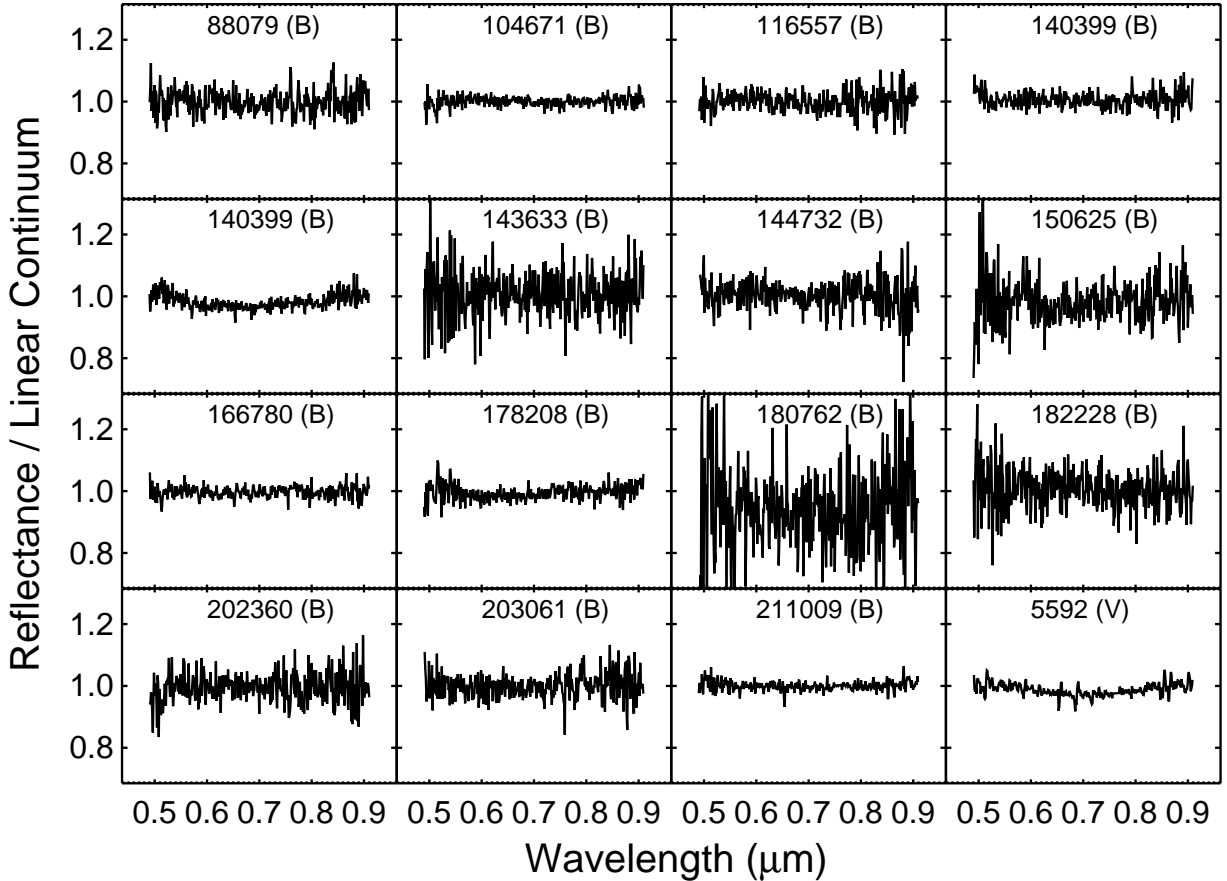


Fig. 3.— Continuum removed spectra of individual asteroids. Labels show the asteroid ID as well as family membership, where (B) and (V) are Beagle and Veritas family members, respectively.

4.2. Hydration Features

Florczak et al. (1999) and Fornasier et al. (2014) suggest that the $0.7 \mu\text{m}$ feature is less frequent among asteroids with decreasing diameters. Data from the SMASS II survey show a high fraction of hydrated members in the young (Nesvorný et al. 2003, 8.3 Myr;) Veritas asteroid family (Bus & Binzel 2002b), so we took spectra of 5 randomly selected small ($D < 10 \text{ km}$) and 2 moderately sized ($D \sim 20 \text{ km}$) Veritas members to test if the $0.7 \mu\text{m}$ feature was observable on small diameter objects. We found 4 out of 7 (57%) asteroids less than 25 km in diameter show the $0.7 \mu\text{m}$ feature. Although asteroid 169282 does not pass our detection criteria (the depth of the band is less than the SNR limits), visual inspection of the spectrum (Fig. 4) does suggest the feature is present. Including asteroid 169282, 3 out of 5 members ($\sim 60\%$) with $D < 15 \text{ km}$ show the $0.7 \mu\text{m}$ feature, suggesting we should expect to detect the feature on small Themis and Beagle asteroids if phyllosilicates were present.

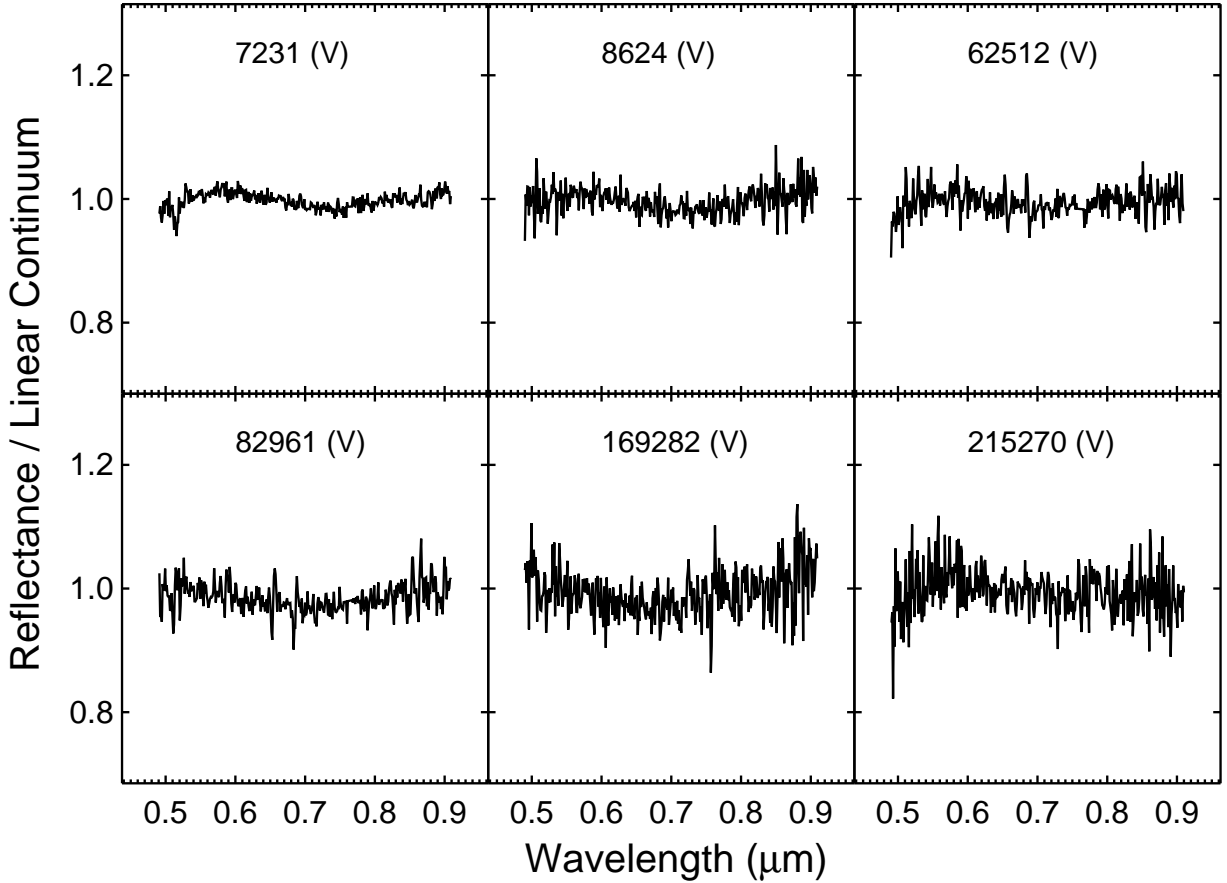


Fig. 4.— Continuum removed spectra of individual Veritas (V) asteroids, where labels report the asteroid ID.

However, only one Beagle (140399) and no Themis asteroids show the feature. It is important to note that asteroid 140399 was imaged on two separate observing runs and only one of the spectra (Fig. 2) shows the absorption. Despite the lack of $0.7 \mu\text{m}$ features in the Themis members, a small number of objects (4 of 22, or 18%) show evidence of the Fe^{2+} UV absorption band also attributed to phyllosilicates (Vilas 1994). A similarly small fraction (3 of 23, or 13%) of the Beagle asteroids also show this UV feature. Due to the cutoff in the spectral coverage below $0.47 \mu\text{m}$, we did not attempt to fit the Fe^{2+} UV feature, but its presence was assessed through visual inspection. Table 2 shows which asteroids were flagged as showing the UV feature.

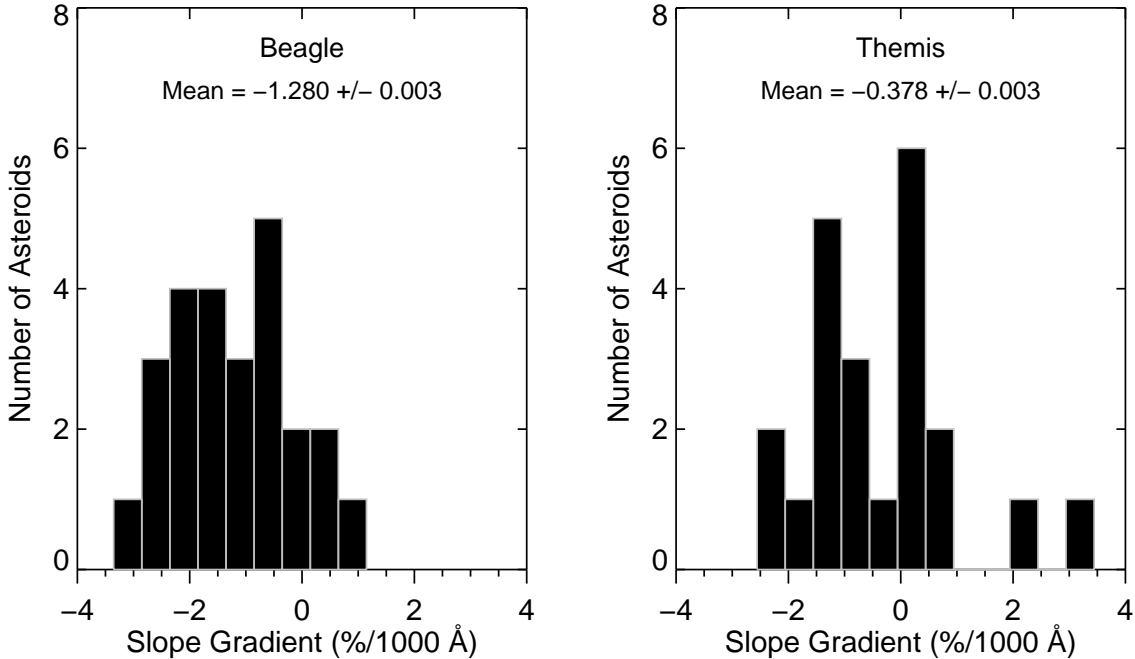


Fig. 5.— Spectral slope gradients (as defined by Jewitt & Meech (1986)) for Themis and Beagle members. The weighted mean and standard error of the mean are reported.

4.3. Albedo Variations

The WISE survey sensitivity is strongly dependent on the distance and diameters of surveyed asteroids. As Beagle and Themis members have nearly identical orbital elements, the detection sensitivity in our analyses is limited to asteroid diameters. Therefore, due to the small size range of the Beagle asteroids, we limit the comparison between the three families to objects with diameters less than 15 km. Figure 6 shows the WISE albedo distributions as function of diameter for both the small ($D \leq 15$ km) and large ($D > 15$ km) asteroid populations in each family. The population of small Themis asteroids have a lower average albedo ($p_v = 0.068 \pm 0.001$) than the Beagle asteroids ($p_v = 0.079 \pm 0.005$). Unexpectedly, the small diameter Veritas asteroids, which are similar in age to the Beagle family, have albedos ($p_v = 0.069 \pm 0.001$) similar to the older Themis asteroids within the same size range. In addition, the larger Themis asteroids ($D > 15$ km) are significantly brighter ($p_v = 0.075 \pm 0.001$) than the smaller members. The Veritas asteroids also show some evidence in albedo variations between small and large members, however the difference is not statistically significant.

For comparison between our results and Masiero et al. (2013), we fit gaussian profiles to the log distributions of the three families. The distributions in log space are shown in Figure 7. We find that our gaussian

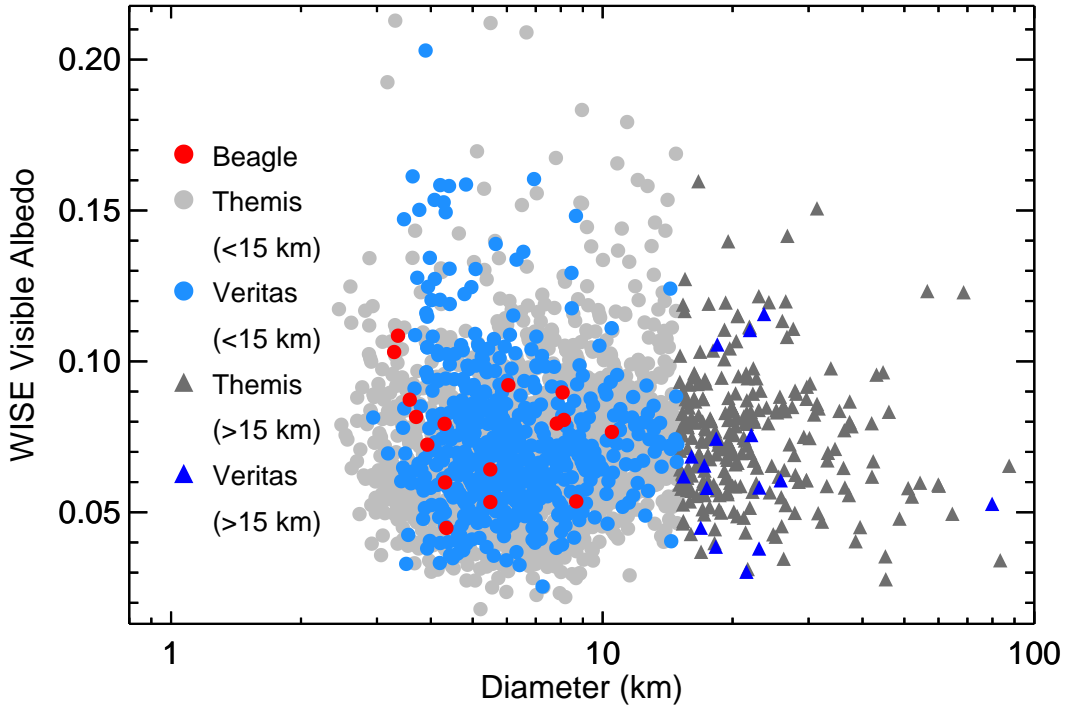


Fig. 6.— WISE albedo distributions for Beagle, Themis and Veritas asteroid families from Masiero et al. (2013).

means are consistent with the values derived by Masiero et al. (2013). When comparing the gaussian medians with the observed sample distribution, we find the gaussian values are slightly larger than the means of the observed population. The difference in means imply the observed population does not follow a gaussian distribution. The apparent non-gaussian distribution may originate from an observational bias introduced by the dependence of WISE derived albedos upon previously published absolute magnitudes (Masiero et al. 2013). However, since the Themis, Beagle and Veritas families are located at similar heliocentric distances, the observational biases are similar for each family, allowing comparison of the observed albedo distributions for these families.

5. Discussion

Spectral characteristics such as slopes and absorption features are one of the few tools available for assessing asteroid compositions remotely. The abundance of the absorber, size distribution of the regolith grains (Clark 1999), and space weathering processes (Conel & Nash 1970; Gold et al. 1970; Hapke et al. 1970) all greatly influence the features of asteroid spectra. Although these processes and characteristics are

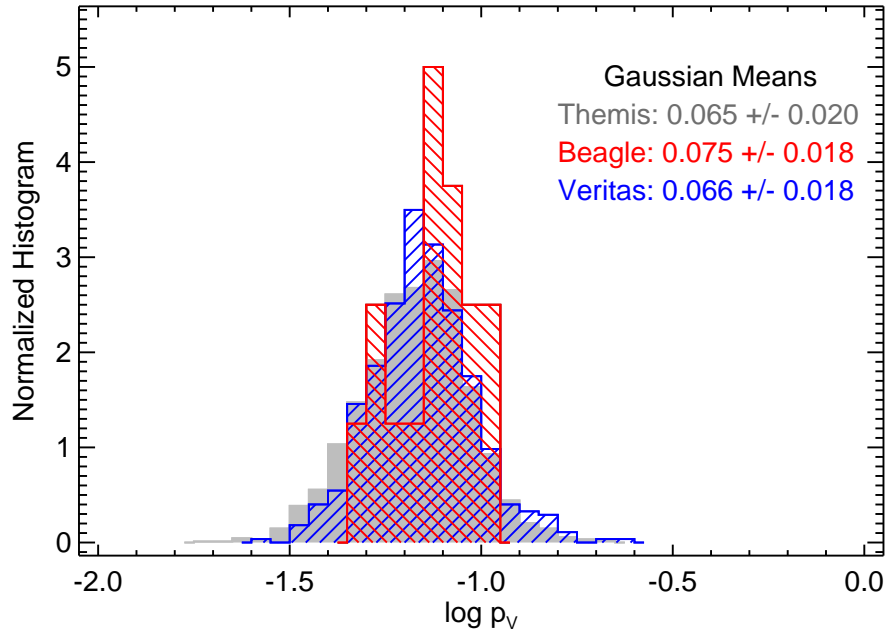


Fig. 7.— Log plot of WISE albedo (p_v) distributions for Themis, Beagles and Veritas asteroids. Each histogram has been normalized to unit area for comparison. Gaussian mean and widths are reported for each family.

difficult to disentangle when analyzing spectroscopic data, the sensitivity of spectroscopy to these processes allows it to be a powerful remote sensing tool.

5.1. C-Complex Space Weathering Trends

As seen in Figure 5, the older Themis asteroids have distinctly redder slopes than the younger Beagle asteroids. This difference implies the spectral slopes of C-complex asteroids become redder over time, which is consistent with the trends observed by Lazzarin et al. (2006). Although the slope evolution of C-complex asteroids appears consistent with silicate-rich asteroids (Nesvorný et al. 2005; Lazzarin et al. 2006), the albedo trends are not. Masiero et al. (2011) find the younger Karin family has a lower albedo than the older Koronis family. In contrast, our data suggest the younger Beagle asteroids have a higher albedo than the older Themis asteroids. Future work is necessary to assess whether the albedo trends in Karin and Koronis are representative of the broad S-complex weathering trends.

The relatively young ages of the Veritas and Beagle asteroids suggest they have minimally evolved regoliths, yet the Veritas asteroids show a much higher fraction (57%) of hydrated members than the Beagle asteroids (13%). Therefore, the low fraction of features in the Beagle asteroids likely reflects an intrinsically

low phyllosilicate content. However, considering the higher fraction (35-60%) of large Themis members with phyllosilicate features (Florczak et al. 1999), we postulate the diagnostic features have been removed due to regolith evolution and space weathering processes. We describe this hypothesis further in § 5.2. In addition to the difference in phyllosilicate features, the Veritas family albedos show that they are darker than the Beagle asteroids, but comparable to the older Themis asteroids. Thus, these data imply a significant difference in the composition between the Veritas and Themis/Beagle families and that the trend observed by Nesvorný et al. (2005) is likely a product of mineralogical variation rather than space weathering processes.

Classical space weathering models attribute the reduced band depths, darkening and reddening of atmosphereless bodies to the optical effects of SMFe particles (Hapke 2001). Although C-complex asteroids appear distinct in their mineralogy when compared to lunar soils and S-complex asteroids (Bus et al. 2002), many of the visible wavelength absorption features in C-complex asteroids are attributed to oxidized Fe transitions (Rivkin et al. 2002, and references within). Thus, the availability of Fe and our observed spectral trends suggest space weathering processes on C-complex asteroids results in the production of SMFe particles.

Using the age difference between the Themis and Beagle families, we estimate a slope increase of $\sim 0.8\%$ per 1000 \AA or $\sim 0.08 \mu\text{m}^{-1}$ in 2.3 Gyr for C-complex asteroids. In comparison, Lazzarin et al. (2006) estimates a weathering rate of $8.8 \pm 4.6 \times 10^{-5} \mu\text{m}^{-1} \text{ AU}^2$ for the C-complex asteroid population, which in 2.3 Gyr equates to $\sim 0.02 \mu\text{m}^{-1}$ for objects with circular orbits located near the Themis asteroids ($\sim 3.1 \text{ AU}$). For S-complex asteroids, Lazzarin et al. (2006) estimates a rate of $24.9 \pm 4.6 \times 10^{-5} \mu\text{m}^{-1} \text{ AU}^2$, corresponding to $\sim 0.06 \mu\text{m}^{-1}$ in 2.3 Gyr for objects at 3.1 AU. Although no estimate was derived for C-complex asteroids, Nesvorný et al. (2005) derive a weathering rate for S-complex asteroids of $0.01 \mu\text{m}^{-1} \times \log_{10} t$ (t given in Myr), which equates to $\sim 0.03 \mu\text{m}^{-1}$ in 2.3 billion years. In contrast, Vernazza et al. (2009) suggests space weathering occurs very rapidly within the main asteroid belt, finding that S-complex asteroid slopes redden by as much as $\sim 0.4 \mu\text{m}^{-1}$ in several million years for newly formed families. A direct comparison between each of these studies is difficult due to the inherent difference in each data set, likely causing the significant difference between each of the estimates. However, our derived rates support the estimates of Lazzarin et al. (2006) and Nesvorný et al. (2005), which suggest that space weathering is a long term process for both S and C-complex main belt asteroids.

5.2. Size Related Spectral Trends

Several groups note trends of a decreased frequency in phyllosilicate absorption features with decreasing size of asteroids (Jones et al. 1990; Vilas & Sykes 1996; Howell et al. 2001; Fornasier et al. 2014). The same trend has been noted in the Themis asteroids in particular, with $\sim 60\%$ of asteroids greater than 50 km presenting phyllosilicate features in contrast to 35% for objects less than 50 km. (Florczak et al. 1999). Additionally, our data show that the fraction reduces to 18% for Themis asteroids with diameters less than 15 km. Furthermore, these size related trends also extend to Themis family albedos, where objects with less than 15 km are darker than larger asteroids.

Due to their lower escape velocities and the inability to retain fine particles during collisions, small asteroids are thought to develop relatively thin regoliths dominated by coarse grains (Matson et al. 1977; Chapman 1978). Indeed, spacecraft observations of small asteroids such as Eros and Itokawa reveal surfaces dominated by gravel and meter sized boulders with fines constricted to low potential zones (Chapman et al. 2002; Miyamoto et al. 2007). These rocky surfaces are hypothesized to be more resistant to gardening processes (Chapman 2002; Willman et al. 2010), thus space weathering effects (decreased albedo and band depths) are likely to be more prevalent on small objects with time. Conversely, impacts upon large asteroids with thicker regoliths and finer particles may be more effective in counteracting space weathering through regolith gardening (Willman et al. 2010), thereby preserving spectral features for longer. Furthermore, laboratory data show that increasing grain size results in a decreased reflectance or albedo and a reduction in absorption band depths (Fischer et al. 1994; Clark 1999; Cloutis et al. 2011a,b). We propose the size related absorption feature and albedo trends in the Themis asteroids originate from the combined effects of coarse grained regoliths and optical maturation times, which result in a pronounced reduction of absorption features and decreased albedos for smaller asteroids.

In contrast to the spectral trends seen in the Themis asteroids, Binzel et al. (1996) found that the small near-Earth asteroids (NEAs) exhibit deeper absorption bands when compared to large NEAs. Chapman (2004) suggests these trends originate from the rapid erosion and resetting of regoliths on smaller asteroids. However, impact velocities are lower in the main belt than the near Earth region (Bottke et al. 2002), thus impact processes will differ between the two populations and may explain the difference in spectral trends with size. Further observations are necessary to assess whether the albedo and absorption feature trends seen in the Themis asteroids are found among other main belt asteroid families.

5.3. Aqueous Alteration in the Themis Parent Body

Several main-belt comets (MBC) (Hsieh & Jewitt 2006) have been dynamically linked to the Themis family (Hsieh 2009; Novaković et al. 2012). The source of sublimation in these MBCs is attributed to water ice buried beneath a layer of regolith several meters thick (Schorghofer 2008; Prialnik & Rosenberg 2009). Thermal evolution models suggest the Themis/Beagle parent body was likely differentiated, with aqueous alteration taking place predominantly in the core, thus allowing the preservation of an icy shell near the surface (Castillo-Rogez & Schmidt 2010; Grimm & McSween 1989; Cohen & Coker 2000).

Due to the young age of the Beagle family and the small fraction of hydrated Beagle members, we believe that the low frequency of features represents an intrinsically low phyllosilicate content in the Beagle parent body. The detection of phyllosilicates in the Beagle asteroids has important implications for geophysical models of the Themis/Beagle parent body, considering the MBC 133P/Elst-Pizarro is a possible member of the Beagle family (Nesvorný et al. 2008). If indeed a member, then the presence of 133P and its volatiles implies the Beagle parent body originated from an ice-rich layer in Themis/Beagle parent body. However, the small but notable fraction of members with the UV and 0.7 μm features suggest the Beagle parent body was not homogeneous, but rather a mixture of ice and aqueously altered material.

We propose two possibilities for heterogeneity of the Beagle parent body. The first is that heterogeneity may represent non-uniform alteration of the Themis/Beagle parent body. Conversely, Rivkin & Emery (2010) and Campins et al. (2010) have potentially detected water ice features on the largest member of the family, 24 Themis. Castillo-Rogez & Schmidt (2010) suggest 24 Themis is the remnant silicate rich core onto which components of its icy crust may have reaccreted following the collisional disruption of the parent body. It is possible the Beagle parent body may be an object which reaccreted non-native components, resulting in the present heterogeneity of the Beagle asteroids. Exploring the viability of these two scenarios is beyond the scope of this paper, however coupled geophysical and dynamical modeling of the two families may provide valuable insights into the evolution of this body.

6. Conclusions

Through comparison of visible spectra and albedo data of the Themis, Beagle and Veritas asteroids, we find the following:

- Space weathering results in an increase of spectral slopes and a decrease in albedo among C-complex asteroids.
- The trends in decreased phyllosilicate features and albedos with decreasing diameter likely result from variations in regolith properties as a function of age and diameter.
- The notable fraction of Beagle members with phyllosilicate features indicate the Beagle parent was a heterogeneous mixture of ice and aqueously altered minerals.
- The apparent mineralogical differences between the Veritas family and the Themis and Beagle families highlight the importance of accounting for mineralogy when interpreting space weathering trends across the broad population of C-complex asteroids.

We would like to say mahalo nui loa to Jan Kleyna, Takashi Hattori and Bin Yang for their help and support of this work. This work is based upon data collected at Subaru Telescope, which is operated by the National Astronomical Observatory of Japan. Image processing in this paper has been performed using the IRAF software. IRAF is distributed by the National Optical Astronomy Observatories, which is operated by the Association of Universities for Research in Astronomy, Inc. under cooperative agreement with the National Science Foundation. Support for this work was provided by the National Aeronautics and Space Administration through the NASA Astrobiology Institute under Cooperative Agreement No. NNA04CC08A issued through the Office of Space Science, by NASA Grant No. NNX07A044G.

REFERENCES

- Belton, M. J. S., Chapman, C. R., Veverka, J., Klaasen, K. P., Harch, A., Greeley, R., Greenberg, R., Head, III, J. W., McEwen, A., Morrison, D., Thomas, P. C., Davies, M. E., Carr, M. H., Neukum, G., Fanale, F. P., Davis, D. R., Anger, C., Gierasch, P. J., Ingersoll, A. P., & Pilcher, C. B. 1994, *Science*, 265, 1543
- Belton, M. J. S., Veverka, J., Thomas, P., Helfenstein, P., Simonelli, D., Chapman, C., Davies, M. E., Greeley, R., Greenberg, R., & Head, J. 1992, *Science*, 257, 1647
- Binzel, R. P., Bus, S. J., Burbine, T. H., & Sunshine, J. M. 1996, *Science*, 273, 946
- Bottke, Jr., W. F., Vokrouhlický, D., Rubincam, D. P., & Broz, M. 2002, *Asteroids III*, 395
- Bowell, E. & Lumme, K. 1979, *Colorimetry and magnitudes of asteroids*, ed. T. Gehrels, 132–169
- Brunetto, R. & Strazzulla, G. 2005, *Icarus*, 179, 265
- Bus, S. J. & Binzel, R. P. 2002a, *Icarus*, 158, 146
- Bus, S. J. & Binzel, R. P. 2002b, *Icarus*, 158, 106
- Bus, S. J., Vilas, F., & Barucci, M. A. 2002, *Asteroids III*, 169
- Campins, H., Hargrove, K., Pinilla-Alonso, N., Howell, E. S., Kelley, M. S., Licandro, J., Mothé-Diniz, T., Fernández, Y., & Ziffer, J. 2010, *Nature*, 464, 1320
- Castillo-Rogez, J. C. & Schmidt, B. E. 2010, *Geophys. Res. Lett.*, 37, L10202
- Chapman, C. R. 1978, in *NASA Conference Publication*, Vol. 2053, NASA Conference Publication, ed. D. Morrison & W. C. Wells, 145–160
- Chapman, C. R. 1996, *Meteoritics and Planetary Science*, 31, 699
- Chapman, C. R. 2002, *Asteroids III*, 315
- Chapman, C. R. 2004, *Annual Review of Earth and Planetary Sciences*, 32, 539
- Chapman, C. R., Merline, W. J., Thomas, P. C., Joseph, J., Cheng, A. F., & Izenberg, N. 2002, *Icarus*, 155, 104
- Clark, R. N. 1999, *Manual of Remote Sensing, Volume 3, Remote Sensing for the Earth Sciences*, ed. A. Rencz, Vol. 3 (John Wiley and Sons), 3–58
- Cloutis, E. A., Hiroi, T., Gaffey, M. J., Alexander, C. M. O. ., & Mann, P. 2011a, *Icarus*, 212, 180
- Cloutis, E. A., Hudon, P., Hiroi, T., Gaffey, M. J., & Mann, P. 2011b, *Icarus*, 216, 309
- Cohen, B. A. & Coker, R. F. 2000, *Icarus*, 145, 369

- Conel, J. E. & Nash, D. B. 1970, *Geochimica et Cosmochimica Acta Supplement*, 1, 2013
- Fischer, E. M., Pieters, C. M., & Pratt, S. F. 1994, in *Lunar and Planetary Science Conference*, Vol. 25, Lunar and Planetary Science Conference, 371
- Florczak, M., Lazzaro, D., Mothé-Diniz, T., Angeli, C. A., & Betzler, A. S. 1999, *A&AS*, 134, 463
- Fornasier, S., Lantz, C., Barucci, M. A., & Lazzarin, M. 2014, *Icarus*, 233, 163
- Gold, T., Campbell, M. J., & O'Leary, B. T. 1970, *Geochimica et Cosmochimica Acta Supplement*, 1, 2149
- Grimm, R. E. & McSween, Jr., H. Y. 1989, *Icarus*, 82, 244
- Hapke, B. 2001, *J. Geophys. Res.*, 106, 10039
- Hapke, B. W., Cohen, A. J., Cassidy, W. A., & Wells, E. N. 1970, *Geochimica et Cosmochimica Acta Supplement*, 1, 2199
- Hirayama, K. 1918, *AJ*, 31, 185
- Hiroi, T., Zolensky, M. E., Pieters, C. M., & Lipschutz, M. E. 1996, *Meteoritics and Planetary Science*, 31, 321
- Howell, E. S., Rivkin, A. S., Vilas, F., & Soderberg, A. M. 2001, in *Lunar and Planetary Science Conference*, Vol. 32, Lunar and Planetary Science Conference, 2058
- Hsieh, H. H. 2009, *A&A*, 505, 1297
- Hsieh, H. H. & Jewitt, D. 2006, *Science*, 312, 561
- Jewitt, D. & Meech, K. J. 1986, *ApJ*, 310, 937
- Jones, T. D., Lebofsky, L. A., Lewis, J. S., & Marley, M. S. 1990, *Icarus*, 88, 172
- Kashikawa, N., Aoki, K., Asai, R., Ebizuka, N., Inata, M., Iye, M., Kawabata, K. S., Kosugi, G., Ohyama, Y., Okita, K., Ozawa, T., Saito, Y., Sasaki, T., Sekiguchi, K., Shimizu, Y., Taguchi, H., Takata, T., Yadoumaru, Y., & Yoshida, M. 2002, *PASJ*, 54, 819
- Lazzarin, M., Marchi, S., Moroz, L. V., Brunetto, R., Magrin, S., Paolicchi, P., & Strazzulla, G. 2006, *ApJ*, 647, L179
- Lumme, K. & Bowell, E. 1981, *AJ*, 86, 1705
- Luu, J. X. & Jewitt, D. C. 1990, *AJ*, 99, 1985
- Mainzer, A., Grav, T., Masiero, J., Hand, E., Bauer, J., Tholen, D., McMillan, R. S., Spahr, T., Cutri, R. M., Wright, E., Watkins, J., Mo, W., & Maleszewski, C. 2011, *ApJ*, 741, 90
- Marzari, F., Davis, D., & Vanzani, V. 1995, *Icarus*, 113, 168

- Masiero, J. R., Mainzer, A. K., Bauer, J. M., Grav, T., Nugent, C. R., & Stevenson, R. 2013, *ApJ*, 770, 7
- Masiero, J. R., Mainzer, A. K., Grav, T., Bauer, J. M., Cutri, R. M., Dailey, J., Eisenhardt, P. R. M., McMillan, R. S., Spahr, T. B., Skrutskie, M. F., Tholen, D., Walker, R. G., Wright, E. L., DeBaun, E., Elsbury, D., Gautier, IV, T., Gomillion, S., & Wilkins, A. 2011, *ApJ*, 741, 68
- Matson, D. L., Johnson, T. V., & Veeder, G. J. 1977, in *Lunar and Planetary Inst. Technical Report*, Vol. 8, *Lunar and Planetary Science Conference*, 625
- Milani, A., Cellino, A., Knežević, Z., Novaković, B., Spoto, F., & Paolicchi, P. 2014, *Icarus*, 239, 46
- Millis, R. L., Bowell, E., & Thompson, D. T. 1976, *Icarus*, 28, 53
- Miyamoto, H., Yano, H., Scheeres, D. J., Abe, S., Barnouin-Jha, O., Cheng, A. F., Demura, H., Gaskell, R. W., Hirata, N., Ishiguro, M., Michikami, T., Nakamura, A. M., Nakamura, R., Saito, J., & Sasaki, S. 2007, *Science*, 316, 1011
- Moroz, L. V., Fisenko, A. V., Semjonova, L. F., Pieters, C. M., & Korotaeva, N. N. 1996, *Icarus*, 122, 366
- Nesvorný, D. 2012, *NASA Planetary Data System*, 189
- Nesvorný, D., Bottke, W. F., Dones, L., & Levison, H. F. 2002, *Nature*, 417, 720
- Nesvorný, D., Bottke, W. F., Levison, H. F., & Dones, L. 2003, *ApJ*, 591, 486
- Nesvorný, D., Bottke, W. F., Vokrouhlický, D., Sykes, M., Lien, D. J., & Stansberry, J. 2008, *ApJ*, 679, L143
- Nesvorný, D., Jedicke, R., Whiteley, R. J., & Ivezić, Ž. 2005, *Icarus*, 173, 132
- Novaković, B., Hsieh, H. H., & Cellino, A. 2012, *MNRAS*, 424, 1432
- Prialnik, D. & Rosenberg, E. D. 2009, *MNRAS*, 399, L79
- Rivkin, A. S. & Emery, J. P. 2010, *Nature*, 464, 1322
- Rivkin, A. S., Howell, E. S., Vilas, F., & Lebofsky, L. A. 2002, *Asteroids III*, 235
- Sasaki, S., Nakamura, K., Hamabe, Y., Kurahashi, E., & Hiroi, T. 2001, *Nature*, 410, 555
- Schorghofer, N. 2008, *ApJ*, 682, 697
- Tholen, D. J. 1984, PhD thesis, University of Arizona, Tucson
- Tody, D. 1986, in *Society of Photo-Optical Instrumentation Engineers (SPIE) Conference Series*, Vol. 627, *Instrumentation in astronomy VI*, ed. D. L. Crawford, 733
- Vernazza, P., Binzel, R. P., Rossi, A., Fulchignoni, M., & Birlan, M. 2009, *Nature*, 458, 993

Vilas, F. 1994, *Icarus*, 111, 456

Vilas, F. & Gaffey, M. J. 1989, *Science*, 246, 790

Vilas, F. & Sykes, M. V. 1996, *Icarus*, 124, 483

Willman, M., Jedicke, R., Moskovitz, N., Nesvorny, D., Vokrouhlicky, D., & Mothé-Diniz, T. 2010, in *Bulletin of the American Astronomical Society*, Vol. 42, AAS/Division for Planetary Sciences Meeting Abstracts #42, 1034

Yamada, M., Sasaki, S., Nagahara, H., Fujiwara, A., Hasegawa, S., Yano, H., Hiroi, T., Ohashi, H., & Otake, H. 1999, *Earth, Planets, and Space*, 51, 1255

Table 1. Observing Geometry and Conditions

Asteroid ID	Vmag	a (AU)	e	i (deg)	r [†] (AU)	Δ [‡] (AU)	α [§] (deg)	Obs Run	No. of Spectra	Airmass (Object)	Solar Analog	Airmass (Stand)
<i>Themis</i>												
7511	17.5	3.205	0.157	1.277	2.694	2.023	6.739	3	2	1.23	HD19061	1.29
8697	18.7	3.106	0.162	0.978	3.606	2.637	3.641	4	2	1.04	HD73708	1.03
15572	18.1	3.209	0.168	2.109	3.030	2.131	9.525	3	2	1.30	HD7983	1.28
15772	19.6	3.217	0.143	2.694	3.530	3.265	16.127	4	2	1.06	HD284013	1.02
16877	17.6	3.055	0.122	1.307	2.726	1.775	7.075	4	2	1.04	HD73708	1.03
18946	19.3	3.046	0.178	0.522	3.181	2.281	8.836	1	1	1.46	HD73708	1.39
26633	18.2	3.220	0.176	2.544	2.702	1.852	12.816	3	2	1.27	HD7983	1.28
28789	18.9	3.132	0.172	0.513	2.857	1.964	10.830	3	2	1.03	HD19061	1.11
31093	17.7	3.135	0.162	3.119	3.144	2.256	9.348	4	2	1.44	G104-335	1.45
31334	17.7	3.176	0.132	1.436	2.807	1.865	7.536	4	2	1.03	HD73708	1.03
38365	18.9	3.198	0.194	2.558	3.275	2.308	4.506	1	1	1.49	BD+30 2047	1.34
47920	18.0	3.126	0.145	2.967	3.186	2.206	3.570	3	2	1.03	HD19061	1.02
51143	18.4	3.146	0.167	1.178	3.139	2.213	8.052	3	2	1.03	HD19061	1.11
51579	19.4	3.166	0.196	2.688	2.610	2.416	22.362	3	2	1.35	HD197081	1.26
54320	17.8	3.116	0.186	0.635	2.543	1.559	3.519	3	2	1.13	HD19061	1.02
58231	17.6	3.222	0.156	2.033	2.735	1.744	1.067	3	2	1.16	HD19061	1.11
58302	18.3	3.097	0.156	1.607	2.710	1.808	10.675	1	1	1.27	HD73708	1.39
82646	18.1	3.061	0.163	3.381	2.692	1.740	7.111	4	2	1.11	HD73708	1.03
91965	18.7	3.244	0.113	1.381	2.977	2.091	10.189	1	1	1.41	HD73708	1.39
123646	18.5	3.227	0.117	2.436	2.901	1.911	1.171	1	1	1.66	HD95868	1.55
132845	20.1	3.122	0.175	1.516	2.580	1.993	20.330	3	2	1.64	HD199011	1.66
149084	19.7	3.180	0.166	2.603	2.676	1.840	13.769	1	1	1.35	HD73708	1.39
<i>Beagle</i>												
7968	20.5	3.157	0.163	1.386	2.856	2.233	17.417	3	2	1.23	HD220764	1.27
8161	17.0	3.167	0.168	2.544	2.778	1.787	1.565	2	2	1.25	HD19061	1.20
	19.2	–	–	–	2.944	3.113	18.518	4	2	1.21	HD19061	1.11
19923	18.5	3.161	0.111	1.698	2.839	2.068	14.693	4	2	1.15	G104-335	1.13
21569	19.2	3.164	0.116	0.676	2.849	2.578	20.266	1	1	1.37	G104-335	1.33
26140	19.2	3.152	0.137	2.545	3.419	2.563	9.435	3	2	1.29	HD7983	1.28
55188	18.6	3.160	0.183	2.453	2.807	2.407	20.152	2	2	1.00	HD73708	1.04
63951	20.2	3.154	0.180	0.454	2.693	2.456	21.632	3	2	1.12	HD73708	1.20
71489	19.7	3.150	0.130	0.781	3.420	2.966	15.844	3	2	1.27	HD603	1.28
84230	20.0	3.157	0.167	0.925	2.911	2.194	15.416	3	2	1.13	HD220764	1.28
88079	19.2	3.151	0.139	0.112	2.761	1.870	10.939	1	1	1.06	HD73708	1.09
104671	19.5	3.162	0.162	0.852	3.061	2.068	0.397	2	2	1.04	HD19061	1.02
116557	20.2	3.161	0.165	1.203	2.934	2.177	14.392	3	2	1.35	HD220764	1.27
140399	20.0	3.146	0.174	1.701	2.705	2.719	21.053	3	2	1.22	HD73708	1.20
	18.7	–	–	–	2.870	1.905	5.227	4	2	1.60	HD95868	1.28
143633	20.1	3.160	0.109	0.755	2.912	2.004	9.276	4	2	1.13	G104-335	1.13
144732	20.6	3.152	0.134	0.435	3.011	2.305	15.249	2	3	1.45	HD284013	1.29
150625	20.3	3.150	0.181	1.353	3.179	2.188	0.077	1	1	1.43	HD95868	1.39
166780	19.1	3.159	0.170	1.343	2.695	1.702	0.866	2	2	1.09	HD19061	1.02
178208	19.8	3.172	0.113	2.565	3.056	2.070	1.835	4	2	1.10	HD95868	1.05
180762	20.9	3.147	0.175	2.183	3.659	2.697	4.341	1	1	1.30	HD95868	1.24

Table 1—Continued

Asteroid ID	Vmag	a (AU)	e	i (deg)	r[†] (AU)	Δ[‡] (AU)	α[§] (deg)	Obs Run	No. of Spectra	Airmass (Object)	Solar Analog	Airmass (Stand)
182228	20.2	3.153	0.170	1.990	3.209	2.240	4.422	1	1	1.09	HD73708	1.09
202360	20.8	3.153	0.132	2.455	3.566	2.579	2.198	2	2	1.33	HD19061	1.20
203061	20.8	3.151	0.157	0.326	3.155	2.167	2.293	3	2	1.30	HD19061	1.11
211009	19.5	3.152	0.132	1.859	2.759	1.782	4.007	4	2	1.33	HD95868	1.28
<i>Veritas</i>												
5592	17.3	3.173	0.062	8.511	3.254	2.696	15.777	3	2	1.05	HD73708	1.03
7231	17.1	3.168	0.075	9.429	2.947	2.215	14.862	3	2	1.20	HD220764	1.28
8624	18.9	3.166	0.032	9.080	3.207	2.384	11.364	4	2	1.04	HD42160	1.14
62512	19.0	3.165	0.065	8.807	3.015	2.040	3.871	4	2	1.05	HD73708	1.03
82961	18.6	3.163	0.057	8.317	3.145	2.163	3.138	3	2	1.09	HD19061	1.02
169282	20.0	3.166	0.082	10.236	3.074	2.536	17.079	4	2	1.04	HD257880	1.02
215270	19.5	3.172	0.079	10.117	2.951	2.027	8.560	2	2	1.15	HD19061	1.20

Note. — Orbital elements (a, e, i) ephemerides, and observational data for each asteroid. Observing run numbers correspond to Run 1= Mar. 02, 2013, Run 2 = Oct. 29, 2013, Run 3 = Oct. 30, 2013, Run 4= Feb. 21, 2014. [†]heliocentric distance [‡]geocentric distance [§]phase angle

Table 2. **Subaru Asteroid Characteristics**

Asteroid ID	Hmag	D ^a (km)	Slope (% / 1000 Å)	SNR ^b	UV ^c Abs	0.7 μm ^c Abs	0.7 μm Band ^d Detection Limit (%)	Obs Run ^e No.
<i>Themis</i>								
7511	13.7	7.09	-0.896 ± 0.020	158.5	Y	N	0.6	3
8697	13.5	9.16	-2.165 ± 0.008	25.0	N	N	4.0	4
15572	13.4	8.12	0.088 ± 0.004	83.6	Y	N	1.2	3
15772	13.4	8.82	-1.917 ± 0.007	40.4	N	N	2.5	4
16877	13.6	9.19	-0.065 ± 0.010	62.5	N	N	1.6	4
18946	14.4	6.36	3.037 ± 0.005	37.0	N	N	2.7	1
26633	14.1	8.06	-0.025 ± 0.004	95.9	Y	N	1.0	3
28789	14.4	6.36	-0.900 ± 0.006	66.0	N	N	1.5	3
31093	13.4	9.43	0.293 ± 0.013	82.6	N	N	1.2	4
31334	13.6	10.18	0.631 ± 0.019	101.5	N	N	1.0	4
38365	14.1	7.79	2.209 ± 0.017	35.4	N	N	2.8	1
47920	13.4	11.25	0.437 ± 0.012	129.7	Y	N	0.8	3
51143	13.4	9.93	-1.083 ± 0.007	79.0	N	N	1.3	3
51579	14.2	6.01	0.807 ± 0.004	33.1	N	N	3.0	3
54320	14.4	7.02	-1.072 ± 0.015	124.0	N	N	0.8	3
58231	14.0	7.64	-1.426 ± 0.012	126.5	N	N	0.8	3
58302	14.2	6.91	-1.473 ± 0.004	71.9	N	N	1.4	1
82646	14.2	6.97	0.115 ± 0.007	50.5	N	N	2.0	4
91965	14.1	6.47	0.250 ± 0.005	55.2	N	N	1.8	1
123646	14.6	5.80	-2.557 ± 0.005	45.8	N	N	2.2	1
132845	15.3	4.24	-0.688 ± 0.007	21.2	N	N	4.7	3
149084	15.0	4.78	-1.161 ± 0.004	27.1	N	N	3.7	1
<i>Beagle</i>								
7968	15.6	4.87	-1.132 ± 0.004	13.5	N	N	7.4	3
8161	13.3	10.51	-1.787 ± 0.004	99.3	N	N	1.0	2
			0.964 ± 0.010	31.2	N	N	3.2	4
19923	13.8	8.08	-0.128 ± 0.008	85.3	N	N	1.2	4
21569	13.9	13.65	0.455 ± 0.015	55.5	N	N	1.8	1
26140	14.1	7.83	0.418 ± 0.004	54.0	N	N	1.9	3
55188	13.6	8.69	-1.924 ± 0.002	32.9	N	N	3.0	2
63951	15.0	5.54	-1.664 ± 0.003	39.6	N	N	2.5	3
71489	13.8	8.13	-0.242 ± 0.003	28.2	N	N	3.5	3
84230	15.1	5.49	-2.572 ± 0.005	32.2	N	N	3.1	3
88079	14.9	5.49	-3.353 ± 0.005	35.6	N	N	2.8	1
104671	15.4	4.36	-1.261 ± 0.003	55.0	N	N	1.8	2
116557	15.2	4.30	-0.810 ± 0.005	33.0	N	N	3.0	3
140399	14.6	6.39	-1.555 ± 0.003	40.7	N	N	2.5	3
			-2.340 ± 0.012	55.8	N	3.4 ± 1.3	1.8	4
143633	15.7	3.53	-0.423 ± 0.011	14.9	N	N	6.7	4

Table 2—Continued

Asteroid ID	Hmag	D ^a (km)	Slope (% / 1000 Å)	SNR ^b	UV ^c Abs	0.7 μm ^c Abs	0.7 μm Band ^d Detection Limit (%)	Obs Run ^e No.
144732	15.6	3.70	-1.082 ± 0.003	17.9	N	N	5.6	2
150625	16.1	3.26	-2.444 ± 0.009	22.0	N	N	4.5	1
166780	15.7	4.09	-2.506 ± 0.004	58.5	N	N	1.7	2
178208	15.6	4.34	-1.895 ± 0.008	41.6	N	N	2.4	4
180762	15.5	3.29	-1.379 ± 0.013	10.8	N	N	9.3	1
182228	15.6	4.34	-0.710 ± 0.008	23.4	N	N	4.3	1
202360	15.6	3.57	-0.469 ± 0.003	21.3	N	N	4.7	2
203061	16.3	3.02	-0.363 ± 0.007	26.3	N	N	3.8	3
211009	15.7	3.98	-2.058 ± 0.010	70.9	N	N	1.4	4
<i>Veritas</i>								
5592	11.7	22.09	-1.366 ± 0.011	111.4	N	3.0 ± 0.7	0.9	3
7231	12.2	18.33	-0.588 ± 0.007	103.9	Y	1.1 ± 0.8	1.0	3
8624	13.6	9.50	0.167 ± 0.002	49.9	N	1.9 ± 1.8	1.9	4
62512	14.7	5.76	1.211 ± 0.013	73.8	Y	1.4 ± 1.1	1.3	4
82961	14.1	6.93	-2.582 ± 0.010	65.7	N	3.0 ± 1.2	1.5	3
169282	14.6	6.27	-0.704 ± 0.006	26.9	N	N	3.7	4
215270	15.1	5.34	1.411 ± 0.002	30.2	N	N	3.3	2

Note. — Spectral data of asteroids observed with Subaru telescope. ^a Diameters (D) were computed using mean family albedos when diameter measurements were not available from WISE. ^b Mean signal to noise ratios, measured using data between $0.49 < \lambda < 0.91 \mu\text{m}$. ^c Indication where absorption is seen in the spectrum either in the UV or at $0.7 \mu\text{m}$. If visible, the $0.7 \mu\text{m}$ band depth is reported. ^d Detection limits derived from the mean signal to noise ratio of each spectrum. ^e Observing runs 1, 2, 3, and 4 correspond Mar. 02, 2013, Oct. 29, 2013, Oct. 30, 2013, and Feb. 21, 2014 respectively.

Table 3. Asteroid Family Characteristics

Family	Slope %/1000 Å	σ_{slope}	Albedo (< 15 km)	σ_{albedo}	Albedo (≥ 15 km)	σ_{albedo}
Beagle	-1.280 ± 0.003	1.080	0.0794 ± 0.0045	0.0179	–	–
Themis	-0.378 ± 0.003	1.342	0.0680 ± 0.0006	0.0236	0.0747 ± 0.0013	0.0214
Veritas	0.196 ± 0.001	1.532	0.0695 ± 0.0010	0.0245	0.0619 ± 0.0064	0.0255

Note. — Slopes represent weighted means for each family, and albedo means were derived from reported WISE values (Masiero et al. 2011). The uncertainty reported with the means are the standard error of the mean. The sigma values represent the standard deviation and show the dispersion for each population.